International Journal of Heat and Fluid Flow 115 (2025) 109833

Contents lists available at ScienceDirect

International Journal of Heat and Fluid Flow

journal homepage: www.elsevier.com/locate/ijhff

Application of turbulent diffusivity models to point-source dispersion in outdoor and indoor flows

H.D. Lim [a,c], Christina Vanderwel [b,*]

[a] Temasek Laboratories, National University of Singapore, Singapore 117411, Singapore
[b] Department of Aeronautics and Astronautics, University of Southampton, Southampton, SO16 7QF, United Kingdom
[c] School of Civil, Aerospace and Design Engineering, University of Bristol, Bristol, BS8 1TR, United Kingdom

ARTICLE INFO

Dataset link: https://doi.org/10.5258/SOTON/D2706, https://doi.org/10.5258/SOTON/D2932

Keywords:
Turbulent diffusivity models
Scalar dispersion
Air pollution
Indoor air quality
Gaussian plume model
Eddy diffusion model

ABSTRACT

The modelling and prediction of scalar transport in turbulent flows is crucial for many environmental and industrial flows. We discuss the key findings of our experimental campaigns which focus on two relevant applications: the scalar dispersion of a ground-level point-source in (1) a smooth-wall turbulent boundary layer flow and (2) a supply-ventilated empty room model. For flows dominated by mean advection, including many outdoor flows, we show how the Gaussian Plume Model provides a good framework to describe the mean scalar field and discuss its limitations in assuming an isotropic and homogeneous turbulent diffusivity. For indoor flows, we explore the balance of the advective and turbulent fluxes and their dependence on the near-source flow field. We use our improved understanding on the scalar transport mechanism in these applications to assess the application of the Eddy Diffusion Model to predict indoor scalar dispersion, and highlight the importance of carefully defining what the turbulent diffusivity coefficient encompasses in different approaches.

1. Introduction

Hazardous air pollutants released in public spaces are a threat to national security and can have long-lasting repercussions on the public health and economy. Managing the consequences of these incidents often requires time-sensitive decisions that are supported by science. As such, it is important to have the capability to model the scalar dispersion of hazardous air pollutants accurately and quickly.

The transport of a scalar quantity from a continuous point-source is challenging to model in turbulent shear flows and can be approached in several ways depending on the application. In the absence of surface deposition or chemical reactions (i.e. negligible sources/sinks) and neglecting molecular diffusion, the mean flow advection and turbulent diffusion are the two dominant processes that can affect the scalar transport. The Reynolds-averaged advection–diffusion equation that describes the mean concentration ($\overline{C}$) of a species is:

$$\frac{\partial \overline{C}}{\partial t} + \underbrace{\overline{U}_i \frac{\partial \overline{C}}{\partial x_i}}_{\text{mean advection}} + \underbrace{\frac{\partial \overline{c' u_i'}}{\partial x_i}}_{\text{turbulent diffusion}} = 0, \tag{1}$$

where c', u_i' and $\overline{U}_i$ represents the concentration fluctuation, velocity fluctuation and mean velocity respectively. The simplest model for dealing with the turbulent scalar fluxes, $\overline{c' u_i'}$, is the Standard Gradient-Diffusion Hypothesis (SGDH) relation which is given as:

$$-\overline{c' u_i'} = D_{ij} \frac{\partial \overline{C}}{\partial x_j}, \tag{2}$$

where D_{ij} is the turbulent (eddy) diffusivity tensor, which reduces to a single coefficient ($K\delta_{ij} = D_{ij}$, where δ_{ij} is the Kronecker delta) in isotropic turbulence. Note that the terms 'turbulent' diffusivity and 'eddy' diffusivity are often used interchangeably in the literature and refer to the same thing. There is a huge body of literature based on the advection–diffusion and SGDH framework. This includes studies on uniformly sheared flow (Vanderwel and Tavoularis, 2014), indoor room flow (van Hooff et al., 2014) and wall-bounded flow (Lim and Vanderwel, 2023). More generally, steady Reynolds-Averaged Navier–Stokes equations (RANS) simulations which do not resolve concentration and velocity fluctuations would have to rely on the turbulent diffusion coefficient as a way to calculate the turbulent scalar fluxes using the mean properties.

For outdoor environmental applications where the mean flow is typically unidirectional, the advection–diffusion equation is an ideal framework for modelling air pollution. In this case, under the assumptions of steady state flow, and that the mean advection dominates the turbulent diffusion in the direction of the mean flow, the analytical

* Corresponding author.
E-mail addresses: hlim022@e.ntu.edu.sg (H.D. Lim), c.m.vanderwel@soton.ac.uk (C. Vanderwel).

https://doi.org/10.1016/j.ijheatfluidflow.2025.109833
Received 7 January 2025; Received in revised form 25 March 2025; Accepted 26 March 2025
Available online 24 April 2025

Nomenclature

Abbreviations

ACH	Air changes per hour
$ADMS$	Atmospheric Dispersion Modelling System
CFD	Computational Fluid Dynamics
$CMOS$	Complementary Metal-Oxide Semiconductor
EDM	Eddy Diffusion Model
GPM	Gaussian Plume Model
PDF	Probability Density Function
PIV	Particle Image Velocimetry
$PLIF$	Planar Laser-Induced Fluorescence
$RANS$	Reynolds-Averaged Navier–Stokes equations
$sCMOS$	Scientific Complementary Metal-Oxide Semiconductor
$SGDH$	Standard Gradient-Diffusion Hypothesis
TBL	Turbulent boundary layer

English Symbols

$\delta_{y,\overline{C}}$	Vertical half-width
$c'u'$	Horizontal turbulent scalar flux
$c'v'$	Vertical turbulent scalar flux
c	Concentration
C_0	Peak concentration
C_s	Source concentration
$\boldsymbol{D}_{ij}$	Turbulent diffusivity tensor
D_{tn}	Normal turbulent diffusivity component contributing to the tangential turbulent scalar flux
D_{tt}	Tangential turbulent diffusivity component contributing to the tangential turbulent scalar flux
D_{yx}	Streamwise turbulent diffusivity component contributing to the vertical turbulent scalar flux
D_{yy}	Vertical turbulent diffusivity component contributing to the vertical turbulent scalar flux
h_{exit}	Height of ventilation outlet
h_{inlet}	Diameter of ventilation inlet
K	Turbulent diffusivity coefficient
K_{arb}	Arbitrary value of turbulent diffusivity coefficient
K_{expt}	Experimentally determined turbulent diffusivity coefficient
L, H, W	Length (x), height (y) and span (z) of room
M	Mass of the pollutant
n	Summation limits to generate image sources
$P1, P2, P3$	Upstream to downstream field of views for the TBL experiment
Q_{dye}	Volume flow rate of dye in TBL experiments
r	Wall reflection terms
Re	Reynolds number
Re_τ	Friction Reynolds number
Re_{inlet}	Reynolds number based on ventilation inlet
Sc	Schmidt number
Sc_t	Turbulent Schmidt number
t	Time
u, v, w	Velocity in the streamwise, vertical and spanwise directions
x, y, z	Streamwise, vertical and spanwise directions
x_0	Virtual origin shift
Y_{depth}	Depth of water in the TBL experiments
Y_{GPM}	Height of source above the ground for Gaussian Plume Model

Greek Symbols

δ	Boundary layer thickness
δ_{ij}	Kronecker delta
λ_f	Air change rate parameter in Eddy Diffusion Model
ν_τ	Turbulent viscosity
σ	Dispersion coefficient

Subscripts and Superscripts

$(\,)'$	Variable fluctuation
$(\,)_i$	Index notation
$(\,)_n$	Normal component
$(\,)_t$	Tangential component
$(\,)_{EDM}$	Eddy Diffusion Model parameter
$(\,)_{FS}$	Full-scale
$(\,)_{GPM}$	Gaussian Plume Model parameter
$\dot{(\,)}$	Flow rate
$\overline{(\,)}$	Time average
$\lvert(\,)\rvert$	Magnitude

solution to the advection–diffusion equation for an elevated point source is given by the reflected Gaussian plume model (GPM) as:

$$\overline{C}(x,y,z) = \frac{\dot{M}}{2\pi\overline{U_{GPM}}\sigma_y\sigma_z} exp\left(-\frac{z^2}{2\sigma_z^2}\right) \times \left[exp\left(-\frac{(y-Y_{GPM})^2}{2\sigma_y^2}\right) + exp\left(-\frac{(y+Y_{GPM})^2}{2\sigma_y^2}\right)\right]. \quad (3)$$

In Eq. (3), $\dot{M}$ represents the mass flow rate of the emission source, $\overline{U_{GPM}}$ is the average plume advection velocity in the prevailing wind direction, Y_{GPM} is the height of the source above the ground, and σ_y and σ_z are the dispersion coefficients (i.e. standard deviation of the Gaussian concentration distribution (Stockie, 2011)) corresponding to the y and z directions. Note that σ_y and σ_z are related to the turbulent diffusivity which will be discussed in greater detail later. The y and z coordinates are defined as the wall-normal (i.e. vertical) and the lateral directions respectively, and are defined as such to be consistent with some of our past studies (Lim and Vanderwel, 2023), which are relevant to the discussions in this manuscript.

Examples of Gaussian models for air quality modelling include the US-EPA model AERMOD (Cimorelli et al., 2005) and the ADMS model developed by the CERC and the UK Meteorological Office (Carruthers et al., 2000). Although this approach is highly popular in outdoor air quality modelling, it relies heavily on empirical estimates of the turbulent diffusivity to control the growth of the scalar plume and decay of the concentration peak. Our previous experimental study on the scalar plume of a point-source in a turbulent boundary layer flow (Lim and Vanderwel, 2023) has shown that the turbulent diffusivity is anisotropic and inhomogeneous. To better understand the

uncertainties resulting from the use of an isotropic and homogeneous turbulent diffusivity coefficient in widely used Gaussian models, it is necessary to perform direct comparisons between the experimental dataset and Gaussian models.

For indoor air quality modelling, the room flow is usually more complex than outdoor flows, since the mean flow patterns are dependent on the air change per hour (ACH) (Cheng et al., 2011), ventilation design and room geometry (Foat et al., 2020). To avoid having to resolve the complex flow patterns or separately resolve the mean flow advection in indoor spaces, an alternative framework is commonly used in indoor airflow applications where there is a lack of dominant flow direction. In this case, the scalar dispersion problem can be modelled using the diffusion equation framework (Fick's second law), which is the same as Eq. (1) but without the mean advection term. Recent studies based on this approach include the experimental study on the repeated passage of a single cylinder in a channel (Mingotti et al., 2020), the continuous release of carbon monoxide in indoor spaces (Cheng et al., 2011) and the determination of the turbulent diffusion coefficient in a mechanically ventilated room using the turbulent kinetic energy balance (Foat et al., 2020).

There are many analytical solutions to the diffusion equation (Fick's second law). For short duration dispersion events in the absence of dominant mean flow advection, the Eddy Diffusion Model (EDM) (Nicas et al., 2009) is given as:

$$C(x,y,z,t) = \frac{M exp(-\lambda_f t)}{(4\pi K_{EDM} t)^{3/2}} r_x r_y r_z, \tag{4}$$

where M is the mass of pollutant released at t=0, λ_f is the air change rate, K_{EDM} is the turbulent diffusivity coefficient, and r_x, r_y and r_z are wall reflection terms, implemented as image sources to satisfy the no-flux wall boundaries (Nicas et al., 2009). The EDM is particularly well-suited for applications where the turbulent diffusion coefficient that controls the net scalar dispersion rate is known (Cheng et al., 2011; Foat et al., 2020). Although it has been shown to be valid in many indoor airflow scenarios (Cheng et al., 2011; Shao et al., 2017; Foat et al., 2020), its accuracy is reliant on selecting the right value of the turbulent diffusion coefficient. Our previous experimental work has shown that the turbulent diffusivity is dependent on several factors, including the air change rate, room ventilation design and source location (Lim et al., 2024). To better understand the performance of the EDM under various flow conditions, direct comparisons between the experimental dataset and the EDM results are needed.

Regardless of indoor or outdoor dispersion applications, the turbulent diffusivity is an important parameter that controls the scalar transport. Although most scalar dispersion models require only a single turbulent diffusion coefficient to predict the concentration of pollutants, Calder (1965) has presented theoretical proof that shows the turbulent diffusivity tensor cannot be diagonal unless the flow turbulence is isotropic. In real-world applications, flow turbulence is rarely isotropic, and measurements of an anisotropic and non-homogeneous turbulent diffusivity tensor have been observed in several different flow applications (Lim and Vanderwel, 2023; Tavoularis and Corrsin, 1985).

In this paper, we examine the application of turbulent diffusivity models to two idealised turbulent flow applications representing outdoor and indoor flows, respectively: the scalar dispersion of a ground-level point-source in (1) a smooth-wall turbulent boundary layer (TBL) and (2) a supply-ventilated empty room model. We compare experimental datasets from our past studies (Lim and Vanderwel, 2023; Lim et al., 2024) to turbulent diffusivity models, and discuss the uncertainties associated with approximating the turbulent diffusivity tensor with an isotropic and homogeneous turbulent diffusion coefficient which is often required for fast running mathematical models. The validity of assumptions made in dispersion models are examined, and their implications on the predicted concentration under various flow conditions are discussed.

2. Methodology

Experiments were performed in a recirculating water tunnel using simultaneous Particle-Image Velocimetry (PIV) and Planar Laser-Induced Fluorescence (PLIF), which enabled velocity and concentration measurements as well as the advective and turbulent mass fluxes. For the outdoor scalar dispersion experiment as illustrated in Fig. 1(a), Rhodamine 6G fluorescent dye (Schmidt number, Sc=2500) was used as a proxy for the pollutant, and was released as a point source in a smooth-wall TBL flow with friction Reynolds number of Re_τ = 2300. The dye flow rate was maintained at Q_{dye}=10 mL min^{-1} to minimise disturbance to the flow, and introduced at ground-level using an embedded 2.5 mm tube with source concentrations (C_s) adjusted to maximise the dynamic range of the PLIF camera. Polyamide seeding particles (50 μm) were added to the flume and recirculated until the desired seeding density and uniformity were achieved. The fluorescent dye and seeding particles were illuminated with a Nd:YAG double-pulsed laser, and wavelength filters were used to separate the PIV and PLIF signals to the cameras. Two 4MP CMOS cameras in a side-by-side configuration and one 5.4MP 16-bit depth sCMOS camera were used for the PIV and PLIF measurements respectively. Experiments were repeated for three field-of-views, P1, P2 and P3, to achieve a combined streamwise field-of-view of around 5.8δ, where δ=104.6 mm was the boundary layer thickness.

For the indoor scalar dispersion experiment as illustrated in Fig. 1(b), a 60:1 full-to-model scale room model with dimensions of 148 mm (H)×445 mm (L)×1200 mm (W) was mounted in an upside down configuration. The ventilation inlet consists of h_{inlet}=60 mm diameter circular holes with 80 mm diameter deflector plates, which allowed the flow to form ceiling jets similar to diffusers (Foat et al., 2020). The outlet was a rectangular slot opening with h_{exit}=33 mm which represents a quasi-2D door with a height of 2 m at full-scale. This room configuration was selected to produce realistic room flows while maintaining a relatively simple room geometry for fundamental studies. The flow was driven by the flume and maintained at a constant velocity to achieve Re_{inlet} = 17,400 and equivalent full-scale air changes per hour (ACH_{FS}) of 1.9 h^{-1}. Rhodamine 6G dye was released as a point source at ground-level at Q_{dye}=10 mL min^{-1} through a 2.5 mm tube. The PIV seeding particles, illumination and image acquisition hardware were the same as the TBL test case.

In both experiments, PIV calibration was performed using a LaVision calibration plate, and post-processing was performed using the LaVision DaVis 10 software. Two PLIF calibration tanks with known dye concentration (within the linear response regime) and the background concentration were used for PLIF calibration, and the PLIF post-processing was performed using in-house codes. The PIV and PLIF resolution for the TBL flow was 0.51 mm and 0.082 mm respectively, while the PIV and PLIF resolution for the indoor room flow was 1.56 mm and 0.174 mm respectively. Joint velocity-concentration statistics were calculated by upsampling the velocity field to the resolution of the concentration field via linear interpolation. The propagated measurement uncertainties of the joint velocity-concentration statistics is estimated to be up to 10.2% at 95% confidence interval for the TBL flow and 14.7% at 95% confidence interval for the room flow respectively. Readers may refer to Lim and Vanderwel (2023) and Lim et al. (2024) for more details on the TBL flow and the room flow experimental procedures respectively.

3. Outdoor dispersion

3.1. Experimental measurements of a point-source in a turbulent boundary layer flow

In a TBL flow, the streamwise scalar transport is dominated by the mean flow advection, while the vertical scalar transport is dominated by the turbulent diffusion mechanism. The mean concentration field

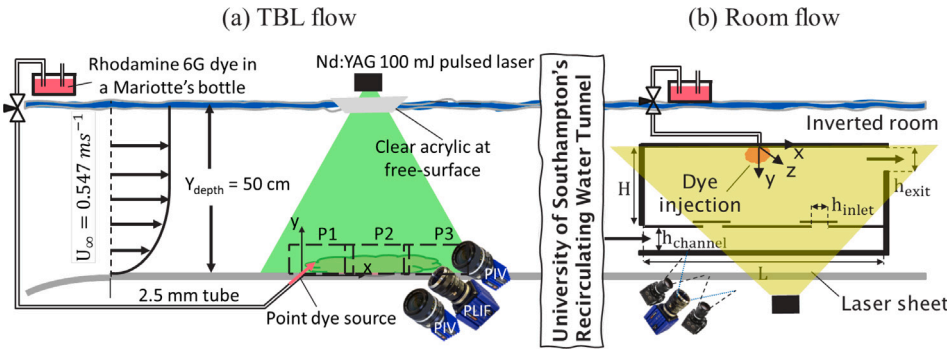

Fig. 1. Schematic of the experimental setup for the (a) TBL flow and (b) the upside down room model. Not drawn to scale, both experiments were performed in separate test campaigns in the University of Southampton's water flume facility. Some elements of the figure have been adapted from Lim and Vanderwel (2023) and Lim et al. (2024).

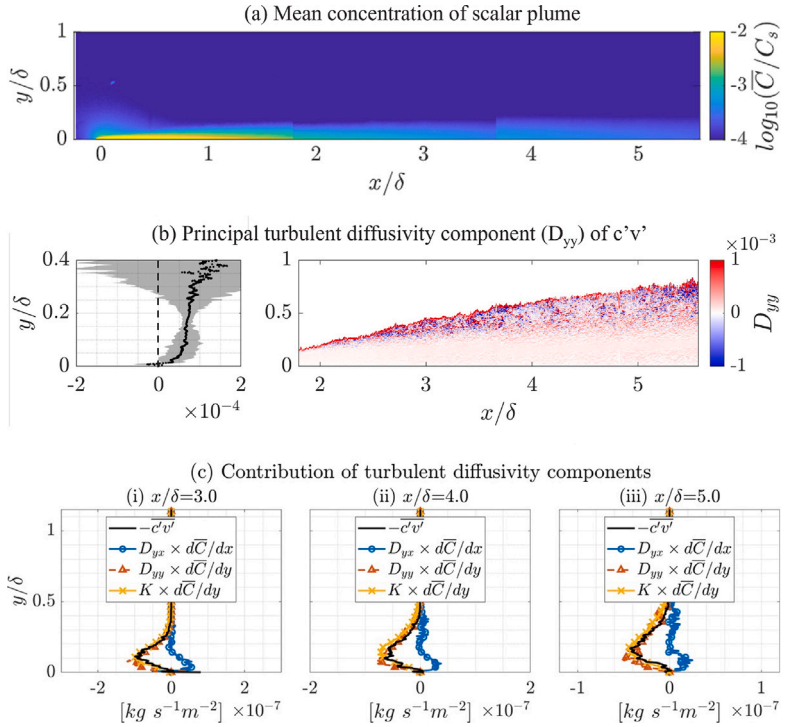

Fig. 2. A continuous point-source in a TBL flow representing an outdoor scalar dispersion problem. Two-dimensional map of the (a) mean concentration of the scalar plume, (b) streamwise-median profile and map of the principal turbulent diffusivity component (D_{yy}) of the wall-normal turbulent scalar flux, and (c) profiles of the contribution of the turbulent diffusivity components to the wall-normal turbulent scalar flux extracted at (i) $x/\delta = 3.0$, (ii) $x/\delta = 4.0$ and (iii) $x/\delta = 5.0$. Some elements of the figure have been adapted from Lim and Vanderwel (2023).

is shown in Fig. 2(a), where the far-field plume exhibits self-similar behaviour, and the concentration vertical profiles (Eq. (5)), plume vertical half-width (Eq. (6)) and the mean peak concentrations decay (Eq. (7)) were observed to follow power-laws (Lim and Vanderwel, 2023):

$$\frac{\overline{C}}{\overline{C_0}} = exp\left[-ln2\left(\frac{y}{\delta_{y,\overline{C}}}\right)^{1.5}\right], \tag{5}$$

$$\delta_{y,\overline{C}}/\delta = 0.065\left(\frac{x-x_0}{\delta}\right)^{0.65}, \tag{6}$$

$$\frac{\overline{C_0}U_\infty\delta^2}{Q_{dye}C_s} = 50\left(\frac{x-x_0}{\delta}\right)^{-1.39}, \tag{7}$$

where $\overline{C_0}$ represents the mean peak concentration, δ represents the boundary layer thickness, x_0 represents a virtual origin shift, and Q_{dye} is the volume flow rate of the pollutant source.

These results are consistent with the literature of the scalar dispersion of a point-source in atmospheric boundary layer flow (Robins, 1978), except for the introduction of the virtual origin shift and slightly different scaling constants. In this case, the tracer dye remains trapped in the viscous sublayer of the smooth-wall TBL, hence a virtual origin shift of x_0=1.3δ was necessary. For the same reason, molecular diffusion and advection of the dye within the viscous sublayer effectively increases the source size and reduces the source strength relative to the logarithmic layer of the TBL flow. Hence, our plume is slightly wider with lower peak concentrations when compared with Robins (1978). In comparison to the GPM, our measured power law exponents show faster plume growth and decay of the peak concentration than the traditional Gaussian plume solution which predicts the plume widths grow as $x^{0.5}$ and the peak concentration decay scales as x^{-1}. This can be attributed to non-constant turbulent diffusion coefficients.

To gain additional insights to the turbulent diffusivity, we used the SGDH model in Eq. (2), and our measurements of the turbulent scalar fluxes and mean concentration gradient, to calculate the different components of the turbulent diffusivity tensor based on the procedure described by Lim and Vanderwel (2023). Two-dimensional maps of the

principal $D_{yy}(x,y)$ component (Fig. 2b) show magnitudes that vary with wall-normal distance. A non-zero cross-diffusivity $D_{yx}(x,y)$ component was also observed due to turbulence anisotropy, which contributed to the vertical turbulent scalar flux in the opposite direction as the $D_{yy}(x,y)$ component (Fig. 2c). Nonetheless, the contribution of $D_{yx}(x,y)$ to the vertical turbulent scalar fluxes was small and the contribution of $D_{yy}(x,y)$ was dominant. As such, it is possible to approximate the turbulent diffusivity tensor using an isotropic turbulent diffusivity coefficient, i.e. $K(x,y) \approx D_{yy}(x,y)$. As shown in Fig. 2c, $K(x,y)$ and the SGDH model was able to provide a good approximation for the vertical turbulent scalar fluxes (i.e. $\overline{c'v'}$) measured in the experiments. Fig. 2(c) also shows that the variation of $K(x,y)$ with wall-normal distance has to be taken into account to accurately reproduce the vertical turbulent mass flux.

3.2. Gaussian plume model

For practical applications, it is important to understand the limitations of the GPM and the associated errors when assuming the turbulent diffusivity is isotropic and homogeneous. Although our experimental results have shown that $K(x,y) \approx D_{yy}(x,y)$ (by assuming isotropic turbulence) is a good approximation to estimate the vertical turbulent scalar fluxes, thus far, we have not addressed the effect of assuming that the turbulent diffusivity is homogeneous, i.e. $K \approx K(x,y)$.

For a ground-level point source (i.e. $Y_{GPM} = 0$), and focusing only on the plume centre-plane (i.e. $z = 0$), the GPM in Eq. (3) can be reduced to:

$$\overline{C}(x,y,0) = \frac{\dot{M}}{\pi \overline{U_{GPM}} \sigma_y \sigma_z} exp\left(-\frac{y^2}{2\sigma_y^2}\right). \tag{8}$$

Eq. (8) still requires an estimate of the dispersion coefficients, σ_y and σ_z, and the mean plume advection velocity, $\overline{U_{GPM}}$, in order to predict $\overline{C}(x,y,0)$. These parameters are not straightforward to estimate even for a smooth-wall turbulent boundary layer in neutral conditions (i.e. no thermal stratification). Hanna et al. (1982) used power laws to define the dispersion coefficients, where the coefficients in the power law are functions of the atmospheric stability class. Melli and Runca (1979) used piecewise power law functions to define the dispersion coefficients and the mean advection velocity for a line source of infinite extent across wind. Liu et al. (2015) used Computational Fluid Dynamics (CFD) simulations to tune the dispersion parameters, and the results were shown to match the CFD results within a factor of 1.5. Stockie (2011) showed that the dispersion coefficients would be related to the turbulent diffusivity as:

$$\sigma^2(x) = \frac{2}{\overline{U_{GPM}}} \int_0^x K_{GPM}(\xi) d\xi. \tag{9}$$

In this study, we consider the special case of isotropic and homogeneous turbulence, hence K_{GPM} is simply a single constant for the entire domain (instead of the more general form of the turbulent diffusivity tensor $D_{ij}(x,y,z)$), and Eq. (9) can be further reduced to:

$$\sigma^2 = \sigma_y^2 = \sigma_z^2 = \frac{2K_{GPM}x}{\overline{U_{GPM}}}. \tag{10}$$

Eq. (8) can therefore be simply expressed as:

$$\overline{C}(x,y,0) = \frac{\dot{M}}{2\pi K_{GPM} x} exp\left(-\frac{y^2 \overline{U_{GPM}}}{4K_{GPM}x}\right). \tag{11}$$

To obtain the mean concentration map using the GPM, we calculated the constant K_{GPM} by taking the streamwise median value of $D_{yy}(x,y)$ over $2.7 < x/\delta < 5.57$ since the scalar plume is fully developed and self-similar for $x/\delta > 2.7$ (Lim and Vanderwel, 2023). We then averaged it over $0.05 < y/\delta < 0.2$ which is an approximation to the vertical half-width of the plume based on the half-maximum of the mean concentration. The value of K_{GPM} that was used to generate the concentration maps for Eq. (11) is $K_{GPM} = K_{expt} = 6.57 \times 10^{-5}$ m^{2}s^{-1}. To better understand the effects of the variations of K_{GPM} on the predicted concentration, we also computed the results for a higher K_{GPM} value by using $K_{GPM} = K_{arb} = 10^{-4}$ m^{2}s^{-1}. As for $\overline{U_{GPM}}$, since the source is at the ground-level, $\overline{U_{GPM}}$ cannot be accurately estimated and would have to be selected somewhat arbitrarily. We estimated the lower bound of $\overline{U_{GPM}}$ using $U(y/\delta = 0.05) = 0.37$ ms^{-1} which is well within the vertical half-width of the plume, and the upper bound of $\overline{U_{GPM}}$ using the freestream velocity (i.e. $U_\infty = 0.55$ ms^{-1}) (Lim and Vanderwel, 2023).

Figs. 3(a) and 3(b) show the mean concentration maps estimated by the GPM using the same value of K_{GPM} but different values of $\overline{U_{GPM}}$, while Figs. 3(b) and 3(c) show the GPM results using different values of K_{GPM} but same values of $\overline{U_{GPM}}$. The choice of the GPM parameter $\overline{U_{GPM}}$ has a limited impact on the mean concentration. In addition, the peak concentration at the ground is constant and not a function of $\overline{U_{GPM}}$, as shown in Fig. 3(d). In contrast, the K_{GPM} parameter has a much more drastic influence on the predicted peak concentration, with a higher value of K_{GPM} leading to lower peak concentration. In comparison to the experiments, the GPM predicts higher peak concentrations by a factor of 3.4 when $K_{GPM} = K_{expt}$. Eq. (11) confirms that the peak concentration, which occurs at the ground, is a function of K_{GPM} and that it decays linearly with downstream distance. As such, the discrepancies between the peak concentration values in the experimental and the GPM results in Fig. 3(d) can be attributed to the selection of the parameter K_{GPM}, which controls the plume growth rate in the vertical and lateral direction.

The experimental results have shown that $K_{GPM}(x,y) = D_{yy}(x,y)$ is able to accurately reproduce the vertical turbulent scalar fluxes. Assuming that the GPM is a suitable dispersion model for outdoor flows, the mismatch in the peak concentrations shown in Fig. 3(d) can be attributed to a combination of the following factors: (1) the lateral dispersion is greater than the vertical dispersion but this cannot be captured by a single coefficient K_{GPM} under the isotropic turbulence assumption, (2) K_{GPM} is a function of both x and y, and using a single value of K_{GPM} that is homogeneous in space has also introduced uncertainties.

Fig. 3(e) shows the mean concentration normalised by the peak concentration $\overline{C_0}$, where $\overline{C_0} = \frac{\dot{M}}{2\pi K_{GPM} x}$. The shape of the normalised concentration profiles is described by the exponential component of Eq. (11). Therefore, it is a function of just the ratio of the mean plume advection velocity and the turbulent diffusivity, i.e. $\overline{U_{GPM}}/K_{GPM}$. In this case, the profiles based on $\overline{U_{GPM}} = U(y/\delta = 0.05)$ and $K_{GPM} = K_{expt}$ (i.e. blue plot) and $\overline{U_{GPM}} = U_\infty$ and $K_{GPM} = K_{arb}$ (i.e. green plot) are similarly close to the experimental data as they have similar $\overline{U_{GPM}}/K_{GPM}$ ratios. Nonetheless, a smaller value of $\overline{U_{GPM}}/K_{GPM}$ is still needed to converge towards the experimental data. An optimal solution for K_{GPM} and $\overline{U_{GPM}}$ exists and can be calculated by performing least squares regression for Eq. (11) with the values of $\overline{C}(x,y)$ obtained from the experiments, similar to how Liu et al. (2015) used CFD results to tune the GPM parameters to achieve an agreement of the results within a factor of 1.5. The main limitation of this approach is that K_{GPM} and $\overline{U_{GPM}}$ are both supposed to be functions of space (Melli and Runca, 1979), hence approximating both of these parameters using single coefficients (understandably so for engineering applications) would inevitably lead to errors in the GPM predictions.

3.3. Relation between scalar and flow turbulence

The relation between the scalar and flow turbulence is important as many CFD simulations (e.g. RANS simulations) rely on the turbulent Schmidt number, Sc_t, and the turbulent viscosity, ν_t, to estimate the turbulent diffusivity coefficient, K. The turbulent Schmidt number, expressed as $Sc_t = \nu_t/K$, is essentially a description of the ratio of the turbulent transport of momentum to the turbulent transport of mass. Using the Boussinesq's turbulent viscosity model and approximating $K(x,y) = D_{yy}(x,y)$, we can calculate the turbulent Schmidt number. Fig. 4(a) shows Sc_t is a function of the wall-normal distance, and

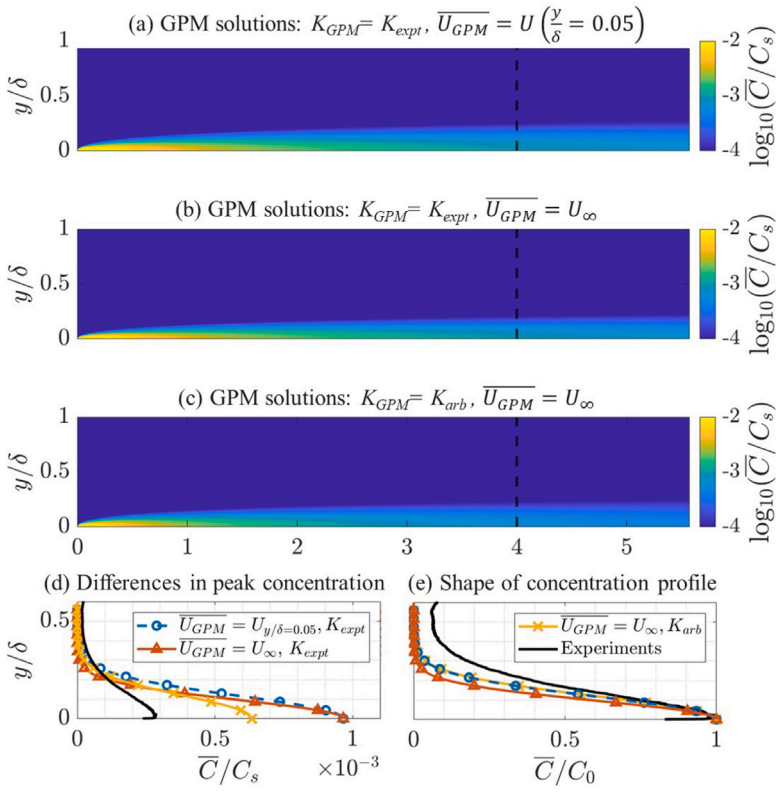

Fig. 3. Mean concentrations from the GPM in the xy-plane using (a) $K_{GPM} = K_{expt}$ and $\overline{U_{GPM}} = U(y/\delta = 0.05)$, (b) $K_{GPM} = K_{expt}$ and $\overline{U_{GPM}} = U_\infty$, and (c) $K_{GPM} = K_{arb}$ and $\overline{U_{GPM}} = U_\infty$. The vertical profiles of the mean concentration extracted at $x/\delta = 4$ (or $(x - x_0)/\delta = 4$), illustrating the differences in the (d) peak concentration and the (e) shape of the concentration profile.

that the peak value of approximately 1.25 occurs at the edge of the logarithmic region of the TBL at $y/\delta = 0.2$. We note that the vertical half-width of the scalar plume based on the half maximum of the mean concentration is close to, but does not exceed, $y/\delta = 0.2$ at $x/\delta = 5$ (Lim and Vanderwel, 2023). A peak value of above 1.0 suggests the flow structures are more effective at transporting the momentum than the scalar. This may be because the tracer scalar is only intermittently present at the plume edge (i.e. around $y/\delta = 0.2$), hence the presence of a vortex may not necessarily transport the scalar, but it will always transport momentum. At $y/\delta > 0.2$, flow turbulence is still present in the flow, but the magnitude of the turbulent scalar flux outside the scalar plume is now much smaller due to the reduction in scalar concentration. Hence, the value of Sc_t decreases to very low values.

The Pearson correlation coefficient map of the Reynolds shear stress and the concentration fluctuation is presented in Fig. 4(b). Large negative values suggest that there is a correlation of Q2 ejection and/or Q4 sweep events with high concentration fluctuation events. Q2 ejection events are characterised by $-u'$ and $+v'$ instantaneous Reynolds shear stress, and imply fluid motion that ejects low momentum fluid from the wall. Q4 sweep events are characterised by $+u'$ and $-v'$ instantaneous Reynolds shear stress, and imply fluid motion that sweeps high momentum fluid towards the wall. Interestingly, at $y/\delta > 0.2$ where the values of Sc_t were previously observed to decrease to very low values, strong negative correlations can still be observed for at least another 0.2δ. This shows that outside the scalar plume, the presence of high concentration fluctuation events can be attributed to Q2 ejection and Q4 sweep events, which are always present as the mechanism to exchange low and high vertical momentum in the TBL. While it is easy to visualise scalars being ejected from the mean plume due to Q2 events, and fresh fluid being swept into the mean plume due to Q4 events, the advection of the scalar due to the mean flow should still dominate the scalar transport mechanism in this specific problem. This has been alluded in an earlier study by Lim and Vanderwel (2023) where they showed that the concentration fluctuation budget is dominated by the advection and dissipation mechanisms.

To better understand this problem, we performed quadrant analysis on the velocity fluctuations at $x/\delta = 4$ and $y/\delta = 0.1$, which is well within the log-layer and the scalar plume, and at $x/\delta = 4$ and $y/\delta = 0.3$, which is outside the log-layer and the vertical half-width of the scalar plume. The velocity fluctuations are plotted as red dots in Fig. 4(c–d). High concentration fluctuation events were identified by using the 98th percentile of the concentration fluctuations, and the velocity fluctuations corresponding to the high concentration fluctuation events are plotted as black dots on the same figure. The percentage textbox in each quadrant in Fig. 4(c–d) represents the ratio of the number of black dots in that quadrant to the total number of black dots in all quadrants.

High concentration fluctuation events can be observed predominantly in Q2, which ranged between 45% and 62.5%, depending on the wall-normal distance. When we apply quadrant hole analysis to focus only on high Reynolds shear stress events, the Q2 quadrant is observed to most likely contain the high concentration fluctuation events (i.e. black dots). This confirms ejection events are predominantly responsible for producing the high concentration fluctuations. Fig. 4(c–d) also shows that the black dots are close to the origin. This shows that high concentration fluctuation events are not necessarily always correlated with large magnitudes of the Reynolds shear stress. In such cases, the advection transport mechanism is most likely responsible for the high concentration fluctuation values, which is consistent with the concentration fluctuations budget analysis performed in an earlier study (Lim and Vanderwel, 2023).

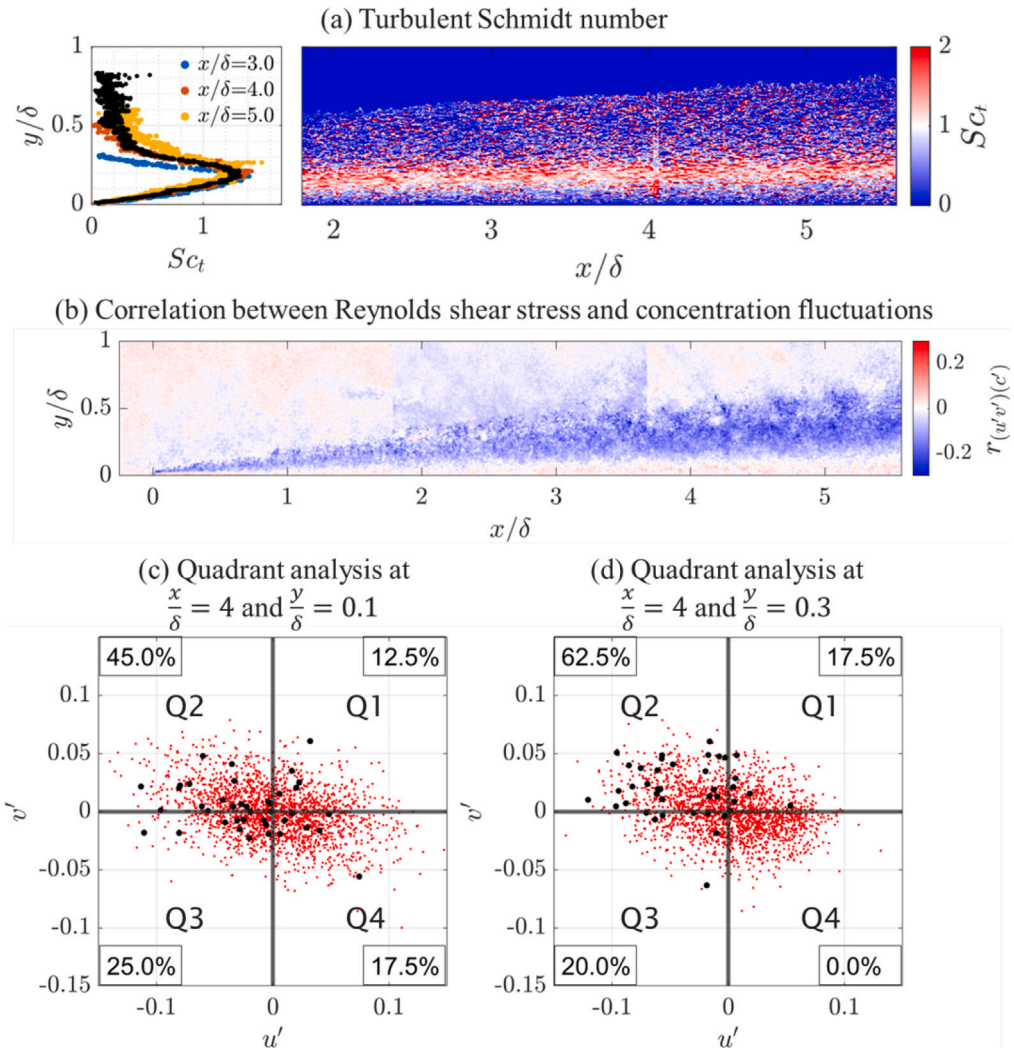

Fig. 4. (a) Profile and map of the turbulent Schmidt number, (b) Pearson correlation coefficient map of the Reynolds shear stress, $u'v'$, with the concentration fluctuations, c', and the quadrant analysis of the velocity fluctuations at $x/\delta = 4$ and (c) $y/\delta = 0.1$ and (d) $y/\delta = 0.3$. The red dots represent the velocity fluctuations of all events, while the black dots represent the velocity fluctuations conditionally sampled based on high concentration fluctuation events (i.e. larger than 98th percentile of the concentration fluctuation PDF). Some elements of the figure have been adapted from Lim and Vanderwel (2023).

4. Indoor dispersion

4.1. Experimental measurements of indoor flow in a scaled room model

In an empty room flow, the flow is considerably more complex as the mean flow direction varies around the room. The mean flow and scalar fields are dependent on several factors, including the air change rate, ventilation design, room geometry and source position within the room (Lim et al., 2024). We illustrate the complexity of indoor mixing using three selected test cases, which have the exact same room geometry and ventilation parameters but with different source positions. As shown in Fig. 5(a)ii, the inflow is at the top and the outflow is at the bottom right, with key dimensions of the room similar to the Nielsen benchmark model (Nielsen, 1990). The ground-level source is at either the middle (Fig. 5i), left (Fig. 5ii) or right (Fig. 5iii) of the room. These three test cases will be named as TC-M, TC-L and TC-R respectively.

The mean velocity vector map in Fig. 5(a)ii (flow field is similar for all three test cases) shows how changing the source location would lead to changes in the near-source flow fields, which have a significant influence on the shape of the mean concentration isocontour lines and scalar dispersion properties as shown in Fig. 5(a). This comparison shows that it is important to understand the flow field in the near-source region, as it affects the initial scalar dispersion patterns and underlying scalar transport mechanism, which would have the largest influence on the overall scalar distribution in the room.

The simultaneous velocity and scalar measurements allow for direct measurements of the in-plane advective and turbulent scalar fluxes (which are shown in detail by Lim et al. (2024)). Fig. 5(b) shows the maps of the ratio of the magnitudes of the turbulent to advective scalar fluxes. The scalar transport mechanism in the near-source region is complex and non-linear, even when the room design and ventilation parameters are the same, and only the source location is varied.

For test cases TC-M and TC-L, the mean flow advection did not introduce significant directivity to the transport of the scalar or dominate the scalar transport mechanism. Rather, the scalar transport is dominated by turbulent diffusion aligned with the mean concentration gradient in the near-source region. This resulted in mean concentration isocontour lines that are relatively semicircular (Fig. 5(a)). For test case TC-R, Fig. 5(b)iii shows the near-source region has advective scalar flux that are at least an order of magnitude greater than the turbulent component (values smaller than −1). The dominance of the mean flow advection introduces significant directivity to the transport of the scalar, thus resulting in mean concentration isocontour lines as shown in Fig. 5(a)iii.

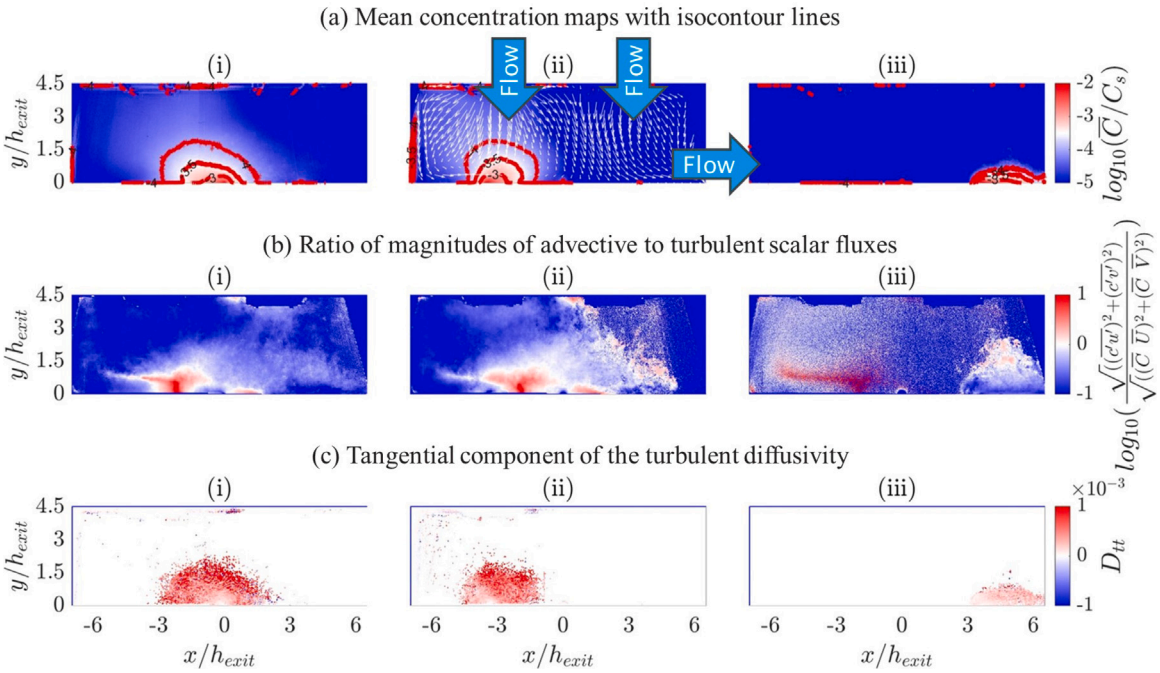

Fig. 5. A continuous point-source in a 60:1 full-to-model scale empty room model representing an indoor scalar dispersion problem. (a) Mean concentration with isocontour lines, (b) ratio of the magnitudes of the advective to turbulent scalar fluxes, (c) tangential component of the turbulent diffusivity (calculated using a different method as the TBL test case). Test cases (i) TC-M (source at x/h_{exit}=0), (ii) TC-L (source at x/h_{exit}=−4.6) and (iii) TC-R (source at x/h_{exit}=4.6). Some elements of the figure have been adapted from Lim et al. (2024).

Since the mean flow is multi-directional in the entire room domain, it makes sense to define the turbulent diffusivity with respect to the direction of the local turbulent scalar flux vector. With this definition, the turbulent scalar flux has a tangential component that is aligned with the vector, and a normal component that is orthogonal to the vector and must therefore be zero. Hence, at every spatial location, the contributions of the concentration gradient to the turbulent scalar flux is simply:

$$-\overline{c'\boldsymbol{u}'}|_t = D_{tt}\frac{\partial \overline{C}}{\partial \boldsymbol{x}}\bigg|_t + D_{tn}\frac{\partial \overline{C}}{\partial \boldsymbol{x}}\bigg|_n, \tag{12}$$

$$-\overline{c'\boldsymbol{u}'}|_n = 0, \tag{13}$$

where D_{tt} and D_{tn} are the tangential and normal turbulent diffusivity components contributing to the tangential turbulent scalar flux. The resulting estimates of D_{tt}, which has a dominant contribution to the turbulent scalar flux shown in Eq. (12), are presented in Fig. 5(c). Since D_{tt} dominates, the turbulent diffusivity coefficient can be estimated using $K \sim D_{tt}$. This method of focusing on the SGDH model may work well for cases TC-M and TC-L, but works less well for case TC-R which is advection-dominated. Additionally, for both TC-M and TC-L cases, this can only be estimated where there are concentration measurements near the source, but one could expect this to be representative of the room domain. The key rationale behind this is that the mean concentration decays very rapidly, by orders of magnitude, with distance from source. As such, small variations/uncertainties in the far field turbulent diffusivity would have a negligible effect on the overall scalar transport predictions. The magnitudes of the estimated turbulent diffusivities are $\mathcal{O}(10^{-3}\ \mathrm{ms}^{-2})$.

The discussions thus far indicate a prior knowledge of the flow field is needed in order to select the most appropriate model to predict concentrations for indoor airflow applications. A caveat to the use of these models is that they are designed with specific assumptions and would therefore have limitations. For instance, the EDM which is based on the diffusion equation assumes negligible flow advection, and the single turbulent diffusion coefficient K_{EDM} used in the model (instead of a turbulent diffusivity tensor as a function of space) assumes isotropic and homogeneous turbulence in the room. The complexity of the indoor airflow means any specific scalar dispersion model would start producing inaccurate results as the scalar transport mechanism changes with the development of the scalar plume. This is exemplified in Fig. 5(a)iii, where the non-linear growth/decay of the vertical height of the plume cannot be accurately captured using any existing models.

Additionally, the assumption of isotropic turbulence and approximating the turbulent diffusivity tensor to a single coefficient may introduce additional uncertainties. In outdoor flows, approximating $K \sim D_{yy}$ and neglecting the contributions of D_{yx} did not introduce significant uncertainties to the vertical scalar transport as shown in Fig. 2(c) (discussed in detail in Lim and Vanderwel (2023)). However, in indoor airflows, flow turbulence can be highly anisotropic, and the contribution of the orthogonal concentration gradient to the turbulent scalar flux in the principal direction may not be insignificant. Lim et al. (2024) experimentally measured the turbulent scalar fluxes and mean concentration gradients in Eq. (2), and showed that although the principal component of the turbulent diffusivity D_{tt} is dominant, by approximating D_{ij} to a single turbulent diffusion coefficient (i.e. $K \sim D_{tt}$) and neglecting the contributions from D_{tn}, this would introduce an average error of around 18% for the test cases that were studied.

4.2. Eddy Diffusion Model

In this section, we focus on the EDM to better understand its limitations, particularly when there is non-negligible mean flow advection, and anisotropic and inhomogeneous turbulence and mean advection. Our implementation of the EDM follows that of Drivas et al. (1996), where the Fick's law solution for an instantaneous source (i.e. Eq. (4)) is integrated over time (Cheng et al., 2011) to account for the use of a continuous source in our experiments:

$$C_{EDM}(x,y,z,t) = \int_0^t \frac{\dot{M}exp(-\lambda_f t)}{(4\pi K_{EDM}t)^{3/2}} r_x r_y r_z dt, \tag{14}$$

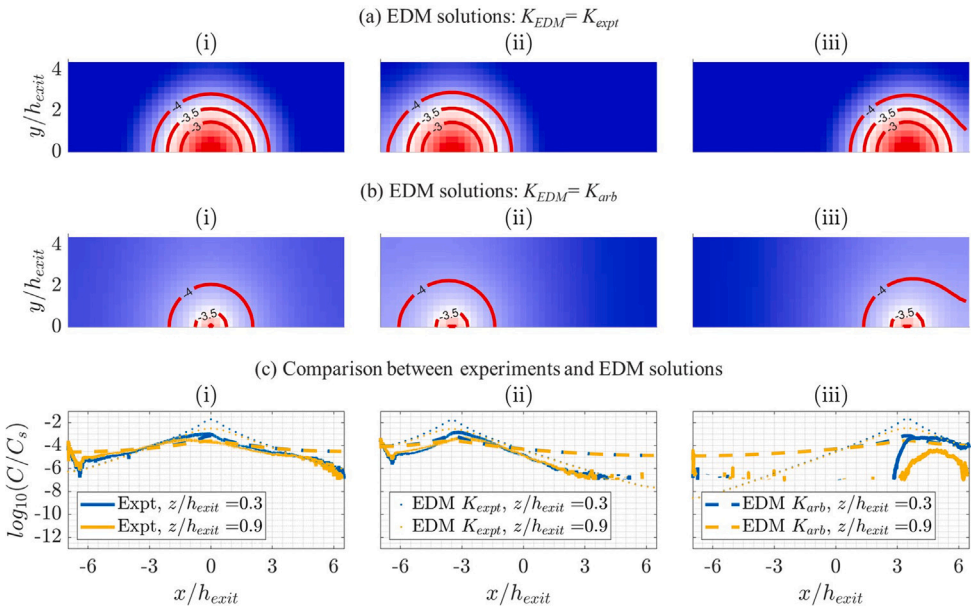

Fig. 6. Solutions to the Eddy Diffusion Model using (a) experimental values of $K_{EDM} = K_{expt}$ (between 8.2×10^{-5} m^2s^{-1} and 1.1×10^{-4} m^2s^{-1}), and (b) $K_{EDM} = K_{arb} = 3\times10^{-3}$ m^2s^{-1}. (c) Comparison between experiments and EDM solutions. Test cases (i) TC-M (source at x/h_{exit}=0), (ii) TC-L (source at x/h_{exit}=−4.6) and (iii) TC-R (source at x/h_{exit}=4.6).

where $\dot{M}$ is the mass emission rate, and the wall reflection terms r_x, r_y and r_z are defined as:

$$r_x = \sum_{n=-\infty}^{\infty}\left[exp\left(\frac{-(x+2nL-x_0)^2}{4K_{EDM}t}\right)+exp\left(\frac{-(x+2nL+x_0)^2}{4K_{EDM}t}\right)\right], \quad (15)$$

$$r_y = \sum_{n=-\infty}^{\infty}\left[exp\left(\frac{-(y+2nH-y_0)^2}{4K_{EDM}t}\right)+exp\left(\frac{-(y+2nH+y_0)^2}{4K_{EDM}t}\right)\right], \quad (16)$$

$$r_z = \sum_{n=-\infty}^{\infty}\left[exp\left(\frac{-(z+2nW-z_0)^2}{4K_{EDM}t}\right)+exp\left(\frac{-(z+2nW+z_0)^2}{4K_{EDM}t}\right)\right], \quad (17)$$

where L, H and W are the dimensions of the room in the respective x, y and z directions. Eq. (14) was implemented using source positions (x_0, y_0, z_0) that corresponded to the experiments. An infinite number of image sources (i.e. $n = \pm\infty$) is not computationally feasible, and usually only a few image sources are needed to achieve sufficiently accurate solutions (Cheng et al., 2011; Foat et al., 2020). Nonetheless, in our case the non-dimensional diffusion time, defined as tK_{EDM}/L^2_{diff} (where L is the distance for the pollutant to diffuse), is relatively large, hence a sufficient number of image sources is still needed. We used $n = \pm5$ as summation limits to create the image sources (i.e. 21 image sources in each direction) to satisfy the no-flux boundary condition at the room walls and t=420 s to achieve steady state solutions — these parameters are selected after ensuring that the solutions have converged.

The EDM solutions presented in Fig. 6(a) are calculated using the turbulent diffusivity values measured from the experiments, which ranged between $K_{EDM} = K_{expt} = 8.2\times10^{-5}$ m^2s^{-1} to 1.1×10^{-4} m^2s^{-1}, depending on the exact test case. Additionally, the EDM solutions for the same conditions, but with $K_{EDM} = K_{arb} = 3\times10^{-3}$ m^2s^{-1} which was arbitrarily selected for the purpose of this discussion, are presented in Fig. 6(b). For test case TC-M and TC-L, Figs. 5(a) and 6(a) are qualitatively comparable, however the line plots in Fig. 6(c) show that the EDM $K_{EDM} = K_{expt}$ solutions have concentration values that are higher than the experimental values in the near-source region. The EDM $K_{EDM} = K_{arb}$ solutions (Fig. 6(b)) are better at matching the concentration values of the experimental data in the near-source region, however they over-predict the concentration values in the far-field region. For the TC-R test case, all EDM solutions are poor and not comparable to the experimental data. There are a few key takeaways regarding EDM based on these observations.

Firstly, to accurately capture the concentration values in the near-source region, K_{EDM} has to be much larger than the experimental measurements of K_{expt}. This is because the EDM is based on the analytical solutions to the diffusion equation, which assumes negligible mean flow advection. In practice, if scalar transport due to mean flow advection is significant (see Fig. 5(b)), then its contribution to the mixing of the scalar has to be consolidated with the turbulent transport. In other words, the value of K_{EDM} used in the EDM model has to compensate for scalar transport due to the mean advection mechanism, i.e. $K_{EDM} = K_{turbulent} + K_{advection}$. Strictly speaking, the turbulent diffusivity term K_{EDM} in diffusion based equations such as Eqs. (4) or (14) is therefore *not the same* as $K\delta_{ij} = \boldsymbol{D}_{ij}$ in Eq. (2) which encompasses only the turbulent transport. They are only equivalent if the scalar transport mechanism due to mean flow advection is truly insignificant.

As an extension of this first point, we would like to highlight how confusion can arise without more careful consideration of the 'turbulent diffusion' terminology. In the indoor airflow literature, estimates of the turbulent diffusion coefficients obtained by matching diffusion-based model predictions to real-world measurements, scaled experiments or high-fidelity CFD data, would inherently combine the scalar transport mechanisms associated with both turbulent diffusion (due to small-scale turbulence) and mean advection (due to mean flow patterns or large-scale flow structure). Strictly speaking, diffusion-based models do not actually ignore the contributions of the mean flow advection if they are present. Instead, they assume the presence of any large-scale flow structures or the mean flow have an isotropic and homogeneous effect on the scalar transport. This would mean a disparity in the turbulent diffusion coefficients obtained based on the advection–diffusion equation approach in comparison to the diffusion-based equations. Currently, there is no discrimination on what the term 'turbulent diffusivity' represents. However, it is important to use different terminologies to avoid ambiguity in the interpretation of the turbulent diffusivity, depending on whether it is based on the advection–diffusion or the diffusion framework. Therefore, we recommend the term 'turbulent diffusion coefficient' (K) for methods based on the advection–diffusion equation approach (Vanderwel and Tavoularis, 2014; Lim and Vanderwel, 2023; Lim et al., 2024) and the term '*total* turbulent diffusion coefficient' (K_{total}) for methods based on the diffusion equation approach (Foat et al., 2020; Cheng et al., 2011; Nicas et al., 2009; Shao et al., 2017).

Secondly, the EDM performs poorly if the scalar transport due to either turbulent diffusion or mean advection is highly anisotropic. The

use of $K_{EDM} = K_{total} = K_{turbulent} + K_{advection}$ would only work well if the scalar transport is isotropic at the room length-scale, such as in test case TC-M and TC-L. If there is highly anisotropic scalar transport, such as in test case TC-R, then the use of K_{total} would not be effective and the EDM solutions would still have very poor agreement to the experimental data (see Fig. 6(c)). The most optimal solution to tackle this would be to either use an anisotropic diffusion-based model (Fischer et al., 2013), or for cases where the mean flow advection completely dominates the scalar transport mechanism (i.e. when sources are close to ventilation inlets or outlets, as shown in Fig. 5(b)iii), switching to the GPM model might be more useful. In practical applications, the drawback to these solutions would be that a prior knowledge of more parameters or the entire flow field are now needed instead of just a single coefficient K_{EDM}. This may not be feasible in applications where fast running mathematical models and solutions are essential.

Thirdly, to accurately capture the concentration values in both near-source and far-field regions, K_{EDM} cannot be homogeneous. As shown in Fig. 6, using $K_{EDM} = K_{arb}$ improves the agreement with the experimental data in the near-source region but it over-predicts the concentration values in the far-field, whereas the converse is true when $K_{EDM} = K_{expt}$. Several studies have evaluated the appropriate values of K_{EDM} for various applications by matching the results of diffusion-based model predictions to real-world measurements, scaled experiments or high-fidelity CFD data (Foat et al., 2020; Cheng et al., 2011; Shao et al., 2017; Karlsson et al., 1994). Our results indicate that if the turbulence and mean flow is inhomogeneous in the room, then the methodology used to estimate K_{EDM} (i.e. position of concentration sensors in experiments or sampling locations in CFD) can result in significant variance in the estimated value of the coefficient.

5. Conclusions

Solutions to scalar dispersion problems in both outdoor and indoor airflow applications rely on the application of turbulent diffusivity models with varying assumptions and boundary conditions. In this study, scalar dispersion experiments were performed for a turbulent boundary layer flow and an indoor flow of a scaled room model. The experimental dataset was used to examine turbulent diffusivity models and understand the limitations of the Gaussian Plume Model and the Eddy Diffusion Model for outdoor and indoor scalar dispersion modelling respectively.

For the outdoor dispersion problem, an isotropic turbulent diffusivity coefficient, $K(x, y) \approx D_{yy}(x, y)$, was shown to be a good approximation to the turbulent diffusivity tensor. Using the SGDH model, and taking into consideration the variation of $K(x, y)$ with wall-normal distance, the vertical turbulent scalar flux could be accurately reproduced. Differences in the peak concentration and normalised concentration profiles estimated by the GPM and the experiments were observed, and was attributed to asymmetric dispersions in the lateral and vertical directions and the use of homogeneous K_{GPM} and $\overline{U_{GPM}}$ coefficients. Finally, Q2 ejection events and mean flow advection were observed to be predominantly responsible for the high concentration fluctuation measurements.

For the indoor dispersion problem, the flow field in the near-source region is of the utmost importance as it determines the underlying scalar transport mechanism in the initial near-source region, which has a large influence on the overall scalar distribution in the room. As such, a prior knowledge of the flow field and the source location is essential to select the most appropriate dispersion model. One of the key assumptions of the Eddy Diffusion Model is negligible mean flow advection. When this assumption is violated, the turbulent diffusivity coefficient used in the EDM has to be much larger to account for the scalar transport due to mean advection, i.e. $K_{EDM} = K_{total} = K_{turbulent} + K_{advection}$. For diffusion-based models, the term K_{total} was introduced to avoid ambiguity, as there is currently widespread use of the same 'turbulent diffusion' terminology in the indoor airflow literature without discrimination on whether the scalar transport model is based on the advection–diffusion or the diffusion equation framework. Finally, the key limitation of the EDM lies in the use of an isotropic and homogeneous turbulent diffusivity coefficient. However, in most practical applications, the airflow in an indoor space is never homogeneous or isotropic even if it is devoid of furniture or human activities. One solution to this may be to use more complex models, such as the anisotropic diffusion-based model or differential methods such as CFD albeit at higher computational cost and time, although this may not be feasible for applications where fast predictions are needed.

There are a few outstanding research questions that we are keen to address in future work. Firstly, the indoor–outdoor pollutant flux has not been considered in this study. With rapid global urbanisation the defining trend of the 21st century, the number of cities and megacities are projected to continue increasing all over the world. This changes the sources/sinks and dispersion properties of air pollutants in the built environment. The indoor–outdoor pollutant flux has a strong influence on air quality and is an extra layer of complexity that needs to be considered. Secondly, pollutant monitors are typically point measurement stations/devices. Sparse pollutant concentration monitors may work well for outdoor applications where there are often existing meteorological data to inform dominant wind patterns and the placement of these monitors. For indoor airflows however, the strong dependence of the mean concentration field on the boundary conditions means selecting the monitor location can be challenging, and multiple (usually wall-mounted) low-cost monitors may be needed to provide representative indoor air quality estimates. Finally, we have not considered the influence of human activities, which can contribute to anthropogenic sources of pollutants or the introduction of turbulence for indoor scalar mixing problems, heterogeneous roughness of city layouts for outdoor pollutant transport, the atmospheric chemistry of primary and secondary (i.e. reactive) pollutants, dry and wet deposition effects, etc. Clearly, the topic of air quality is very diverse, and would benefit from multi-disciplinary approaches to the research problem.

CRediT authorship contribution statement

H.D. Lim: Writing – review & editing, Writing – original draft, Visualization, Validation, Software, Resources, Project administration, Methodology, Investigation, Funding acquisition, Formal analysis, Data curation, Conceptualization. **Christina Vanderwel:** Writing – review & editing, Software, Resources, Methodology, Investigation, Funding acquisition, Conceptualization.

Declaration of competing interest

The authors declare the following financial interests/personal relationships which may be considered as potential competing interests: Christina Vanderwel reports financial support was provided by UK Research and Innovation. H.D. Lim reports financial support was provided by Royal Academy of Engineering. Christina Vanderwel is an associate editor of the International Journal of Heat and Fluid Flow. If there are other authors, they declare that they have no known competing financial interests or personal relationships that could have appeared to influence the work reported in this paper.

Acknowledgements

The authors gratefully acknowledge the support of C.V.'s UKRI Future Leader's Fellowship (MR/S015566/1) and H.D.L.'s Royal Academy of Engineering Intelligence Community Postdoctoral Research Fellowship (ICRF2122-5-184).

Data availability

Experimental data are made available in the University of Southampton data repository at https://doi.org/10.5258/SOTON/D2706 and https://doi.org/10.5258/SOTON/D2932.

References

Calder, K.L., 1965. On the equation of atmospheric diffusion. Q. J. R. Meteorol. Soc. 91 (390), 514–517.

Carruthers, D.J., Edmunds, H.A., Lester, A.E., McHugh, C.A., Singles, R.J., 2000. Use and validation of ADMS-urban in contrasting urban and industrial locations. Int. J. Environ. Pollut. 14 (1–6), 364–374.

Cheng, K.C., Acevedo-Bolton, V., Jiang, R.T., Klepeis, N.E., Ott, W.R., Fringer, O.B., Hildemann, L.M., 2011. Modeling exposure close to air pollution sources in naturally ventilated residences: Association of turbulent diffusion coefficient with air change rate. Environ. Sci. Technol. 45 (9), 4016–4022.

Cimorelli, A.J., Perry, S.G., Venkatram, A., Weil, J.C., Paine, R.J., Wilson, R.B., Lee, R.F., Peters, W.D., Brode, R.W., 2005. AERMOD: A dispersion model for industrial source applications. Part I: General model formulation and boundary layer characterization. J. Appl. Meteorol. Clim. 44 (5), 682–693.

Drivas, P.J., Valberg, P.A., Murphy, B.L., Wilson, R., 1996. Modeling indoor air exposure from short-term point source releases. Indoor Air 6 (4), 271–277.

Fischer, H.B., List, J.E., Koh, C.R., Imberger, J., Brooks, N.H., 2013. Mixing in Inland and Coastal Waters. Elsevier.

Foat, T.G., Drodge, J., Nally, J., Parker, S.T., 2020. A relationship for the diffusion coefficient in eddy diffusion based indoor dispersion modelling. Build. Environ. 169, 106591.

Hanna, S.R., Briggs, G.A., Hosker Jr., R.P., 1982. Handbook on Atmospheric Diffusion. Technical Report DOE/TIC-11223; ON: DE82002045, National Oceanic and Atmospheric Administration, Oak Ridge, TN (USA). Atmospheric Turbulence and Diffusion Lab.

van Hooff, T., Blocken, B., Gousseau, P., van Heijst, G.J.F., 2014. Counter-gradient diffusion in a slot-ventilated enclosure assessed by LES and RANS. Comput. & Fluids 96, 63–75.

Karlsson, E., Sjöstedt, A., Håkansson, S., 1994. Can weak turbulence give high concentrations of carbon dioxide in baby cribs? Atmos. Environ. 28 (7), 1297–1300.

Lim, H.D., Foat, T.G., Parker, S.T., Vanderwel, C., 2024. Experimental investigation of scalar dispersion in indoor spaces. Build. Environ. 250, 111167.

Lim, H.D., Vanderwel, C., 2023. Turbulent dispersion of a passive scalar in a smooth-wall turbulent boundary layer. J. Fluid Mech. 969, A26.

Liu, X., Godbole, A., Lu, C., Michal, G., Venton, P., 2015. Optimisation of dispersion parameters of Gaussian plume model for CO_2 dispersion. Environ. Sci. Pollut. Res. 22, 18288–18299.

Melli, P., Runca, E., 1979. Gaussian plume model parameters for ground-level and elevated sources derived from the atmospheric diffusion equation in a neutral case. J. Appl. Meteorol. Clim. 18 (9), 1216–1221.

Mingotti, N., Wood, R., Noakes, C.J., Woods, A.W., 2020. The mixing of airborne contaminants by the repeated passage of people along a corridor. J. Fluid Mech. 903, A52.

Nicas, M., Keil, C., Simmons, C., Anthony, T., 2009. Turbulent eddy diffusion models. Math. Model. Estim. Occup. Expo. Chem. 53–65.

Nielsen, P., 1990. Specification of a Two-Dimensional Test Case: (IEA). In: Gul Serie, no. 8, Institut for Bygningsteknik, Aalborg Universitet, International Energy Agency, Energy Conservation in Buildings and Community Systems, Annex 20. Air Flow Pattern within Buildings PDF for print: 22 pp..

Robins, A.G., 1978. Plume dispersion from ground level sources in simulated atmospheric boundary layers. Atmospheric Environ. (1967) 12 (5), 1033–1044.

Shao, Y., Ramachandran, S., Arnold, S., Ramachandran, G., 2017. Turbulent eddy diffusion models in exposure assessment-determination of the eddy diffusion coefficient. J. Occup. Environ. Hyg. 14 (3), 195–206.

Stockie, J.M., 2011. The mathematics of atmospheric dispersion modeling. Siam Rev. 53 (2), 349–372.

Tavoularis, S., Corrsin, S., 1985. Effects of shear on the turbulent diffusivity tensor. Int. J. Heat Mass Transfer 28 (1), 265–276.

Vanderwel, C., Tavoularis, S., 2014. Measurements of turbulent diffusion in uniformly sheared flow. J. Fluid Mech. 754, 488–514.